



## Enhanced photocatalytic performance of ZnO/Cu<sub>2</sub>O composite for the degradation of methylene blue under the synergy effect

HONGYING LI<sup>1,2</sup>, LUWEN MA<sup>1</sup>, ZHENYANG WU<sup>1</sup> and CHENGLI YAO<sup>1\*</sup>

<sup>1</sup>School of Chemistry and Pharmaceutical Engineering, Hefei Normal University, Hefei, Anhui, China and <sup>2</sup>Hefei National Research Center for Physical Sciences at the Microscale, University of Science and Technology of China, Hefei, Anhui, China

(Received 15 November, revised 27 November 2025, accepted 29 January 2026)

**Abstract:** In order to investigate the catalytic degradation efficiency of ZnO/Cu<sub>2</sub>O composite, the nanocomposite was synthesized *via* one-pot method and the template of SDS. The crystal structure, microscopic morphology, chemical composition, specific surface area, pore size distribution and optical absorption property of the composite were characterized. Under the irradiation of xenon lamp, the photocatalytic performance of the composite was evaluated by degrading methylene blue (MB). The aforementioned characterization showed that the synthesized composite consisted of ZnO (hexagonal wurtzite) and Cu<sub>2</sub>O (cubic crystal). Due to the mediation of SDS template, the particles were nanoscale with uniform distribution of Cu, Zn and O elements and contained abundant mesopores. The photo-response range of the composite expanded to the visible region because of the combination of ZnO and Cu<sub>2</sub>O. Degradation ratio of MB catalyzed by ZnO/Cu<sub>2</sub>O maintained about 92 % within 100 min after five recycling, demonstrating promising potentiality for photocatalytic applications. The enhanced photocatalytic performance maybe related to the mediation of SDS during the preparation process and the synergy effect between ZnO and Cu<sub>2</sub>O.

**Keywords:** SDS; template; ZnO/Cu<sub>2</sub>O; photocatalytic degradation.

### INTRODUCTION

In recent years, wastewater pollution has increasingly become serious with the rapid development of industrialization. Dyes, pesticides, antibiotics and other organic pollutants which are difficult to degrade in wastewater critically threaten the safety of water ecosystem and human health. Photocatalytic degradation, as a high-efficiency and environment-friendly wastewater treatment technology, has attracted much attention in recent years.<sup>1–4</sup> ZnO,<sup>5,6</sup> CdS,<sup>7</sup> WO<sub>3</sub>,<sup>8</sup> TiO<sub>2</sub>,<sup>9</sup> Cu<sub>2</sub>O,<sup>10</sup> SnO<sub>2</sub>,<sup>11</sup> *etc.*, have once been selected as semiconductor photocatalysts to degrade organic

\* Corresponding author. E-mail: yaochengli@hfnu.edu.cn  
<https://doi.org/10.2298/JSC251115005L>



pollutants in wastewater; however, the photocatalytic performance of a single catalyst is not good. Taking  $\text{Cu}_2\text{O}$  as an example, as a p-type semiconductor with a narrow band gap ( $E_g = 2.1$  eV), it was once considered as a potential photocatalyst because of its low price, environmental friendliness and absorption of most visible light.<sup>10</sup> However, the electron-hole pairs generated in  $\text{Cu}_2\text{O}$ , after absorbing light energy, were easy to recombine quickly. Moreover,  $\text{Cu}_2\text{O}$  was easy oxidized in humid environment, so its photocatalytic performance was unsatisfactory.<sup>12</sup> To improve the photocatalytic performance of  $\text{Cu}_2\text{O}$ , the deposition of metals,<sup>12</sup> doping of nonmetallic elements,<sup>13</sup> recombination with other materials<sup>14</sup> or construction of heterojunction<sup>15</sup> were selected.

As an n-type semiconductor with wide band gap ( $E_g = 3.37$  eV), ZnO has attracted significant attention in recent years by virtue of good chemical stability, convenient preparation method, non-toxicity and low price.<sup>5,6,16</sup> However, as a photocatalyst, ZnO can only be excited by ultraviolet light with high energy, which results in the low utilization efficiency for sunlight and limits its wide application in photocatalytic field. Relevant literature suggested that the photocatalytic property of the composite through combining ZnO with  $\text{Cu}_2\text{O}$  was improved significantly. On one hand, the absorption spectrum of the composite declared a red shift, which significantly improved the availability of sunlight. On the other hand, the separation of photo-generated  $e^-$  and  $h^+$  was effectively promoted due to the energy level matching of two semiconductor materials.<sup>17,18</sup>

Surfactants were often used as soft templates to effectively control the morphology and enhance the dispersibility of materials.<sup>19,20</sup> Up to now, the preparation and photocatalytic performance of ZnO/ $\text{Cu}_2\text{O}$  composite have been studied,<sup>17,18,21–23</sup> but it is rarely reported that surfactants are used as templates to regulate the formation of ZnO/ $\text{Cu}_2\text{O}$ . So, it is worth exploring sodium dodecyl sulfate (SDS) mediating the morphology and structure of ZnO/ $\text{Cu}_2\text{O}$  as well as its properties. Here, ZnO/ $\text{Cu}_2\text{O}$  composite was prepared via one-pot method with the template of SDS. The molecules of SDS self-assembled to form ordered aggregates with specific structures, its hydrophilic groups attracted metal ions, thereby changed the distribution of metal ions in the reaction system. Due to the mediation of SDS template, the composite composed of flower-like nano-ZnO and  $\text{Cu}_2\text{O}$  nano-spheres was prepared, which exhibited satisfactory photocatalytic degradation performance of MB under simulated sunlight. This provided a facile way for the preparation of economical and efficient photocatalysts for wastewater treatment.

## EXPERIMENTAL

### Chemicals

Sodium hydroxide (NaOH, AR), glucose ( $\text{C}_6\text{H}_{12}\text{O}_6$ , AR), sodium dodecyl sulfate (SDS) ( $\text{C}_{12}\text{H}_{25}\text{SO}_4\text{Na}$ , AR), zinc acetate dihydrate ( $\text{Zn}(\text{CH}_3\text{COO})_2 \cdot 2\text{H}_2\text{O}$ , AR), copper acetate monohydrate ( $\text{Cu}(\text{CH}_3\text{COO})_2 \cdot \text{H}_2\text{O}$ , AR), methylene blue ( $\text{C}_{16}\text{H}_{18}\text{N}_3\text{ClS}$ , AR) and absolute ethanol ( $\text{C}_2\text{H}_5\text{OH}$ , AR). Deionized water was used in the whole experiment.

#### *Preparation of ZnO/Cu<sub>2</sub>O with SDS as a template*

1.5 g SDS was added into a beaker containing the mixed solution of Zn(CH<sub>3</sub>COO)<sub>2</sub> (0.5 mol/L, 50 mL), Cu(CH<sub>3</sub>COO)<sub>2</sub> (0.5 mol/L, 50 mL) and glucose (1 mol/L, 25 mL). The beaker was placed in a water bath (60 °C) and kept magnetic stirring for 30 min. Later, NaOH solution (2 mol/L, 50 mL) was added into it drop by drop. The mixing process was assisted by magnetic stirring and lasted for 30 min. The sediment at the bottom of the beaker was collected by centrifugation. It was washed alternately by water and ethanol three times each, and dried under vacuum at 60 °C. The desired sample was prepared and named as S1.

#### *Preparation of ZnO/Cu<sub>2</sub>O, ZnO and Cu<sub>2</sub>O*

For comparison, ZnO/Cu<sub>2</sub>O, ZnO and Cu<sub>2</sub>O without SDS were also synthesized. The following procedure described the synthesis steps. The preparation of ZnO/Cu<sub>2</sub>O composite without SDS mediating was similar as S1, except that SDS was not added. The obtained sample was labeled as S2. 50 mL of Zn(CH<sub>3</sub>COO)<sub>2</sub> solution (0.5 mol/L) was placed in the water bath (60 °C). Then 25 mL of NaOH solution (2 mol/L) was added into it drop by drop with magnetic stirring for 30 min. Then, the white precipitation was centrifuged, washed, and dried in an oven (60 °C) for 24 h. The obtained sample was named as ZnO (S3). 50 mL of Cu(CH<sub>3</sub>COO)<sub>2</sub> (0.5 mol/L) and 25 mL of glucose (1 mol/L) were mixed with a water bath (60 °C). After 10 min of magnetic stirring, 25 mL of NaOH solution (2 mol/L) was added into the mixture drop by drop with a continuous stirring. 30 min later, the brick red precipitation was centrifuged, washed and dried under vacuum. Then, it was collected and named as Cu<sub>2</sub>O (S4).

#### *Characterization*

The crystal structure was characterized using an X-ray powder diffractometer (XRD, TD-3500). The morphology and elemental mapping of the samples were examined using scanning electron microscope (SEM, SU1510; Zeiss Sigma 360) coupled with an energy dispersive spectrometer (EDS). The X-ray photoelectron spectroscopy (XPS) was analyzed by Thermo Scientific K-Alpha spectrometer. The specific surface area was measured by automated surface area and porosimetry analyzer (Micromeritics ASAP 2460). The UV-Vis-DRS absorption spectra were performed using spectrometer (U3900).

#### *Photocatalytic degradation of MB*

Using methylene blue (MB) as a model organic pollutant and a xenon lamp as a simulated sunlight source, photocatalytic degradation experiments were carried out according to the procedure.<sup>6</sup> In short, 150 mg of photocatalysts were put into MB solution (150 mL, 2.0×10<sup>-5</sup> mol/L) with magnetic stirring continuously for 1 h in dark environment. After that, the mixed solution was irradiated by a xenon lamp with the light intensity of 100 mW/cm<sup>2</sup>. The distance of lamp and solution was 15 cm. The degradation solution (1 mL) was taken out every 20 min and centrifuged in the dark. The absorbance of supernatant was monitored by an UV-Vis spectrophotometer in the wavelength range of 550–750 nm. The total illumination time was 100 min. The degradation ratio *R* was calculated as:

$$R(\%) = 100 \frac{A_0 - A_t}{A_0} \quad (1)$$

*A*<sub>0</sub> and *A*<sub>*t*</sub> represent the initial and time-dependent absorbance of MB at 664 nm, respectively.

## RESULTS AND DISCUSSION

*Material characterizations*

The XRD patterns of the four samples are shown in Fig. 1. For comparison, the standard powder diffraction files of Cu<sub>2</sub>O with cubic crystal structure (PDF#65-3288) and ZnO with hexagonal wurtzite structure (PDF#36-1451) were also presented. Fig. 1a is the XRD pattern of S4 sample. The diffraction peaks (marked with \*) matched well with those of cubic Cu<sub>2</sub>O (PDF#65-3288), indicating that sample S4 was Cu<sub>2</sub>O with cubic crystal structure. The XRD pattern of sample S3 is displayed in Fig. 1b. Comparison with the standard powder diffraction file for hexagonal wurtzite ZnO (PDF#36-1451) indicated that the diffraction peaks (marked with ♦) corresponded to hexagonal wurtzite ZnO in sample S3.

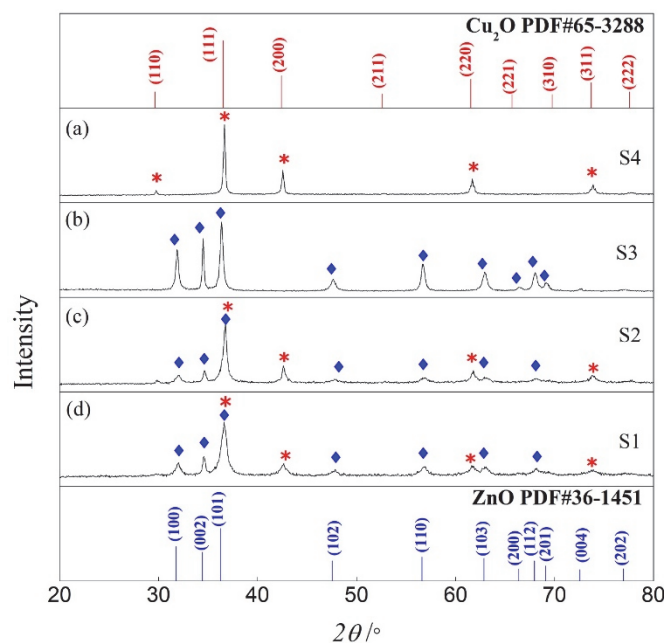


Fig. 1. The XRD patterns of samples: S4 (a), S3 (b), S2 (c) and S1 (d).

Fig. 1c and d are the XRD patterns of S1 and S2 samples. The characteristic diffraction peaks (marked with ♦) corresponded to the (100), (002), (101), (102), (110), (103) and (112) crystal planes of ZnO with wurtzite structure, respectively. At the same time, the peaks at  $2\theta$  36.6, 42.5, 61.6 and 73.9° (marked with \*) matched with (111), (200), (220) and (311) crystal planes of cubic Cu<sub>2</sub>O. These evidences confirmed that the samples of S1 and S2 were the composite of ZnO/Cu<sub>2</sub>O. Moreover, the crystal structure of the component was unchanged under the

mediation of SDS. In addition, there were no other diffraction peaks in Fig. 1a–d, and the sharp peaks declared the synthesized samples were with good crystallinity.

Fig. 2 is the XPS spectra of the ZnO/Cu<sub>2</sub>O (S1) composite. The survey spectrum (Fig. 2a) indicated that Zn, O and Cu elements existed in the composite. In the line spectrum of Zn 2p (Fig. 2b), two dominant peaks at 1021.8 and 1044.7 eV, were attributed to the Zn 2p<sub>3/2</sub> and Zn 2p<sub>1/2</sub> of Zn<sup>2+</sup>, respectively.<sup>24</sup> In the XPS data of O 1s (Fig. 2c), the first peak located at 530.4 eV, corresponding to the lattice oxygen in ZnO and Cu<sub>2</sub>O,<sup>13,25</sup> the second peak appeared at the binding energy of 531.7 eV might be attributed to hydration.<sup>25,26</sup> As shown in Fig. 2d, two binding energy peaks of Cu 2p were observed at 932.4 and 952.3 eV, and ascribed to those of Cu 2p<sub>3/2</sub> and Cu 2p<sub>1/2</sub> from Cu<sup>+</sup> in Cu<sub>2</sub>O, respectively.<sup>13,27,28</sup> In addition, two satellite peaks located at 942.3 and 962.1 eV of Cu(II) were identified, indicating the existence of CuO.<sup>29</sup> However, it is worth mentioning that no characteristic peaks of CuO were detected in the XRD pattern of sample S1, demonstrating that not much Cu<sub>2</sub>O was oxidized to CuO on the surface of the composite. It might be due to the surface sensitivity of the XPS characterization technique. In summary, the characterization of XPS demonstrated the successful synthesis of ZnO/Cu<sub>2</sub>O (S1) composite.

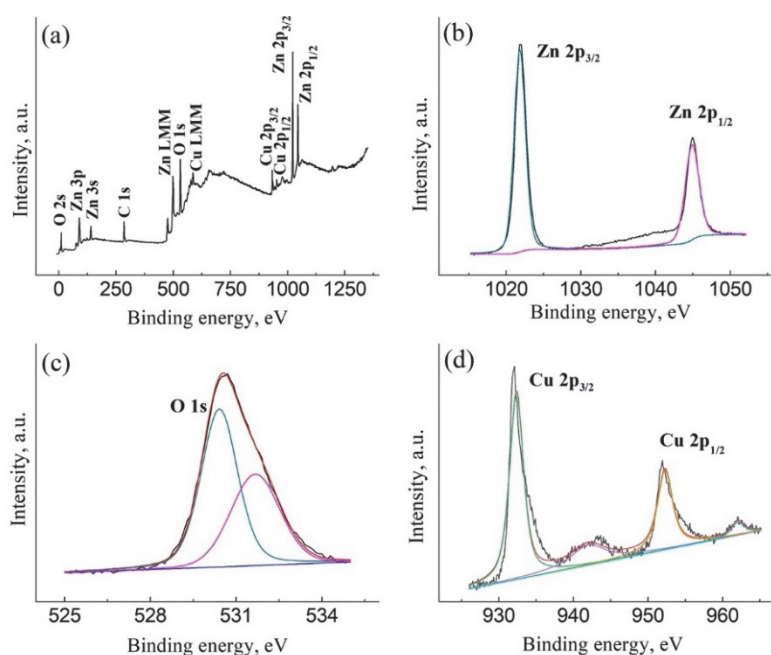


Fig. 2. The XPS spectra of ZnO/Cu<sub>2</sub>O (S1): survey spectrum (a), Zn 2p (b), O 1s (c), Cu 2p (d).

Fig. 3 revealed the SEM images of ZnO, Cu<sub>2</sub>O, ZnO/Cu<sub>2</sub>O(S2) and ZnO/Cu<sub>2</sub>O (S1), together with the EDS spectra and elemental mapping images of

ZnO/Cu<sub>2</sub>O (S1). It can be observed that the morphologies of ZnO particles were irregular, which sizes were in the range of 0.2–1 μm (Fig.3a). Cu<sub>2</sub>O particles, ranging from 0.5 to 2.5 μm, exhibited polyhedral or spherical shapes with smooth surfaces (Fig.3b). For ZnO/Cu<sub>2</sub>O(S2) composite (Fig.3c), it could be seen that ZnO particles adhered to the surface of Cu<sub>2</sub>O, in which, the morphology and size of Cu<sub>2</sub>O particles showed little change compared to the pure Cu<sub>2</sub>O particles (Fig. 3b). Fig. 3d–f displayed that the composite of ZnO/Cu<sub>2</sub>O (S1) was consisted of nano-spherical Cu<sub>2</sub>O aggregates and flower-like ZnO particles. The aggregates of Cu<sub>2</sub>O were formed by the self-assembly of Cu<sub>2</sub>O particles with a size of 50–100 nm. The size of nano-spherical Cu<sub>2</sub>O aggregates was obviously smaller than that of Cu<sub>2</sub>O shown in Fig. 3b. Moreover, the size and morphologies of ZnO particles underwent significant changes comparing with pure ZnO (Fig.3a). Through Fig. 3d–f, it could be found that the particle size of ZnO with flower morphology was about 200 nm.

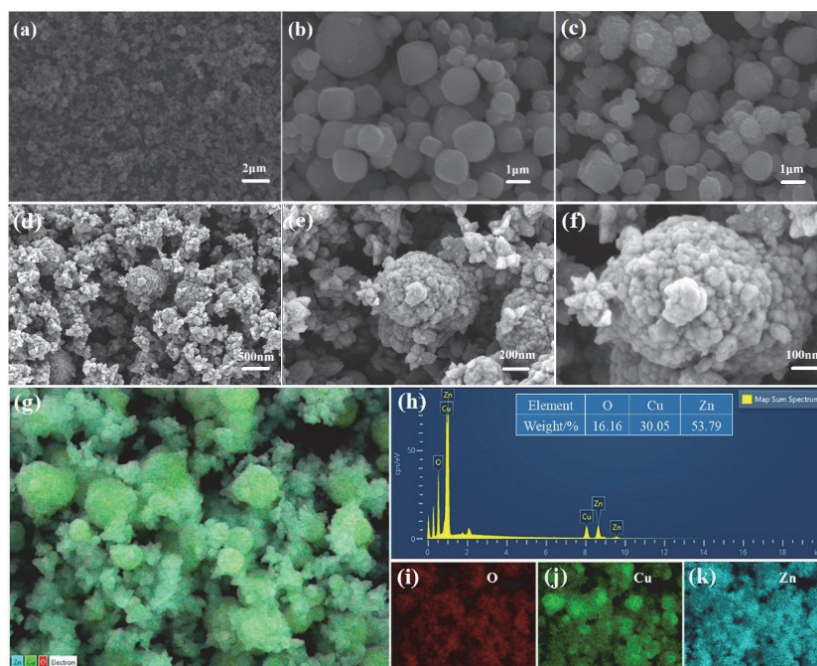


Fig. 3. SEM images of ZnO (a), Cu<sub>2</sub>O (b), ZnO/Cu<sub>2</sub>O (S2) (c), ZnO/Cu<sub>2</sub>O (S1) (d–f); EDS spectra (g–h) and elemental mapping images (i–k) of ZnO/Cu<sub>2</sub>O (S1).

From the EDS spectra (Fig. 3g–h), the elements of Cu, Zn, and O were detected, and no other additional elements were found, which confirmed the composition of ZnO/Cu<sub>2</sub>O (S1) composite. Additionally, it could be seen that Cu, Zn and

O elements (Fig. 3i–k) were uniformly distributed which further verified the successful synthesis of ZnO/Cu<sub>2</sub>O (S1) composite with high purity.

The change of particle size and morphology of ZnO/Cu<sub>2</sub>O (S1) composite was closely related to the regulation of SDS. As a surfactant, the molecules of SDS could form self-assembly aggregates with unique spatial structure when its concentration reached a specific value. These aggregates with obvious structural interfaces could act as soft template to induce the formation of the materials with specific structures, morphologies, and properties. The hydrophilic group of SDS were negatively charged and attracted Zn<sup>2+</sup> and Cu<sup>2+</sup> to gather around them by electrostatic attraction.<sup>30,31</sup> Then, the distributions of metal cations in the solution were changed, and the crystal nucleation sites were regulated. Due to the template effect, the crystal underwent a controlled growth. The structure and morphology of the obtained sample were shaped and the desired property was endowed.

Fig. 4a displayed the N<sub>2</sub> adsorption–desorption isotherm of ZnO/Cu<sub>2</sub>O (S1) composite. The curve accorded with typical type IV isotherm and displayed an obvious hysteresis loop of type H3, indicating the presence of a large number of mesopores.<sup>32</sup> The specific surface area measured by BET method was 17.15 m<sup>2</sup>/g. The pore size distribution calculated by BJH method was shown in Fig. 4b. The average pore diameter was 11.98 nm. The mesoporous channels can facilitate the diffusion of reactant molecules into the interior of the material, which endow the composite with the advantage of adsorption for pollutants and then enhance its photocatalytic performance.

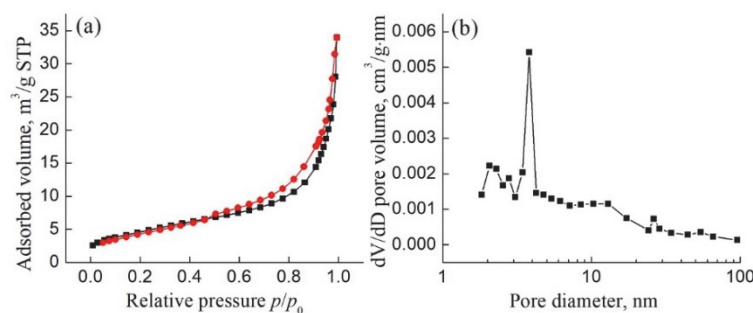


Fig. 4. N<sub>2</sub> adsorption–desorption isotherm (a) and pore size distribution (b) of ZnO/Cu<sub>2</sub>O (S1).

Fig. 5a showed the UV–Vis–DRS absorption spectra of ZnO, Cu<sub>2</sub>O and ZnO/Cu<sub>2</sub>O (S1). It can be observed that ZnO/Cu<sub>2</sub>O (S1) exhibited strong adsorption in the region from 400 to 800 nm. Comparing with ZnO, the photo-response range expanded to the visible region. According to the Kubelka–Munk transformation and Tauc formulas,<sup>33–35</sup> the band gap energies ( $E_g$ ) of ZnO, Cu<sub>2</sub>O and ZnO/Cu<sub>2</sub>O(S1) were calculated and displayed in Fig. 5b. The  $E_g$  value of Cu<sub>2</sub>O and ZnO were approximately 1.99 and 3.25 eV, respectively, which were basically

consistent with previous reports.<sup>27,32</sup> Two  $E_g$  values of 2.06 and 3.22 eV existed for ZnO/Cu<sub>2</sub>O (S1) composite. The  $E_g$  value of Cu<sub>2</sub>O in the composite was 2.06 eV, which was larger than that of pure Cu<sub>2</sub>O (1.99 eV), it lowered the recombination rate of  $e^-/h^+$ .<sup>33</sup> At the same time, the  $E_g$  value of ZnO in the composite was 3.22 eV, instead of 3.25 eV of pure ZnO, the narrowing of the band gap induced the red-shift of the absorption edge.<sup>32</sup> The changes of band gap energy were attributed to successful incorporation of ZnO and Cu<sub>2</sub>O in the composite, which resulted in the enhancement of photocatalytic properties.

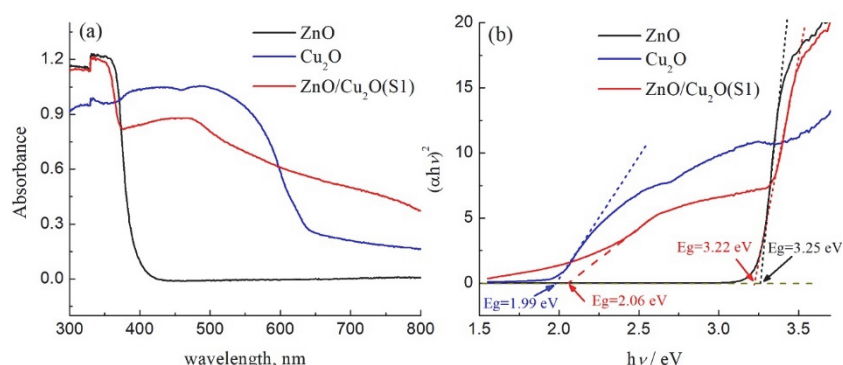


Fig. 5. The UV-Vis-DRS absorption spectra (a) and Tauc plot (b) to calculate the band gap energy.

#### Photocatalytic activity and stability analysis

Fig. 6 presented the UV-Vis spectra of MB solution which underwent photocatalytic degradation by the photocatalysts of ZnO/Cu<sub>2</sub>O (S1), ZnO/Cu<sub>2</sub>O (S2), ZnO and Cu<sub>2</sub>O after different times, respectively. The absorbance values of the solution decreased at the wavelength of 664 nm (the maximum absorption peak of MB<sup>36–38</sup>) with the elapse of illumination time, which suggested that MB was degraded gradually.

To present the photocatalytic performance more intuitively, the degradation ratio  $R$  was calculated and shown in Fig. 7a. The results showed the relationship of  $R$ :  $R(\text{ZnO/Cu}_2\text{O (S1)}) > R(\text{ZnO/Cu}_2\text{O (S2)}) > R(\text{ZnO}) > R(\text{Cu}_2\text{O})$ . Taking 100 min as an example, the degradation ratio  $R$  of MB by ZnO/Cu<sub>2</sub>O (S1) reached 98.1 %, while  $R$  of MB by ZnO/Cu<sub>2</sub>O (S2), ZnO and Cu<sub>2</sub>O were only 80.8, 70.0 and 36.0 %, respectively. Therefore, the photocatalytic efficiency of ZnO/Cu<sub>2</sub>O (S1) was the best among the four photocatalysts.

In order to evaluate the degradation kinetics of MB by the synthesized photocatalysts, the curves of  $\ln(A_0/A_t)-t$  were plotted and shown in Fig. 7b. There was a good linear relationship between  $\ln(A_0/A_t)$  and the time of  $t$ , which accorded with the kinetic characteristics of pseudo first-order. The kinetic parameters of the fitting curves were summarized in Table I. From the data, it was demonstrated that

the  $k$  value of the degradation reaction using ZnO/Cu<sub>2</sub>O (S1) as the photocatalyst was about 2.4, 3.2 and 8.3 times that of ZnO/Cu<sub>2</sub>O (S2), ZnO and Cu<sub>2</sub>O, respectively. Therefore, the ZnO/Cu<sub>2</sub>O (S1) nanocomposite presented an ideal degradation efficiency under the same conditions, demonstrating promising potentiality for photocatalytic applications.

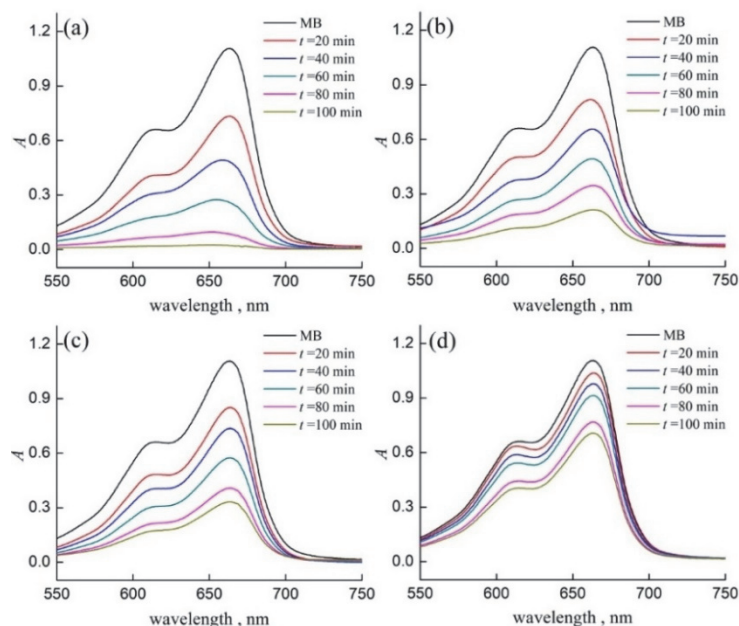


Fig. 6. The UV-Vis spectra of MB solution degraded by ZnO/Cu<sub>2</sub>O (S1) (a), ZnO/Cu<sub>2</sub>O (S2) (b), ZnO (c) and Cu<sub>2</sub>O (d).

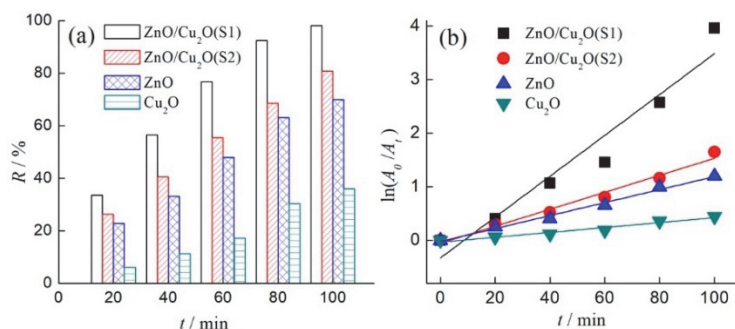


Fig. 7.  $R-t$  histogram (a) and the kinetic curves (b) of photocatalytic degradation of MB.

The enhanced photocatalytic performance of ZnO/Cu<sub>2</sub>O (S1) may be attributed to the mediation of SDS and the synergistic effect of ZnO and Cu<sub>2</sub>O components in the composite. The results of SEM suggested that the morphology of both

TABLE I. Parameters of kinetic curves

Sample	Rate constant $k / \text{min}^{-1}$	$R^2$
ZnO/Cu <sub>2</sub> O (S1)	0.03814	0.92797
ZnO/Cu <sub>2</sub> O (S2)	0.01585	0.97676
ZnO	0.01210	0.98707
Cu <sub>2</sub> O	0.00457	0.94903

ZnO and Cu<sub>2</sub>O changed in shape as in size and became smaller. The BET characterization revealed that the average pore diameter was 11.98 nm. The changes of morphology and particle size, as well as the abundant presence of meso-pores in the composite were closely related to the template effect of SDS. It might make it easier to contact with the molecules of MB and offer more surface adsorption sites, and then facilitate the further occurrence of oxidative decomposition. In addition, another important factor could not be ignored. The energy level matching of Cu<sub>2</sub>O and ZnO in the composite promoted the separation of photo-generated charge carriers electron(e<sup>-</sup>)/hole(h<sup>+</sup>) pairs,<sup>17,33,38</sup> and then improved its catalytic ability. The possible mechanism was described,<sup>17,23,33,39</sup> and the corresponding mechanism diagram was shown in Fig. 8. The e<sup>-</sup> in the valence band (VB) of Cu<sub>2</sub>O and ZnO transferred to the conduction band (CB) under the irradiation of light, and the h<sup>+</sup> was left in the VB. Because the CB position of Cu<sub>2</sub>O is higher than that of ZnO, the photo-generated e<sup>-</sup> in the CB of Cu<sub>2</sub>O transferred to the surface of ZnO; at the same time, the h<sup>+</sup> in the VB of ZnO transferred to the surface of Cu<sub>2</sub>O, thus effectively avoiding the recombination of e<sup>-</sup> and h<sup>+</sup> on the catalyst surface. h<sup>+</sup> and e<sup>-</sup> with strong oxidation and reduction ability react with H<sub>2</sub>O and O<sub>2</sub>, respectively, to form reactive hydroxide radicals (•OH) and superoxide radical anion (O<sub>2</sub><sup>-•</sup>), in which, O<sub>2</sub><sup>-•</sup> can further turn into •OH.<sup>13,24,27,33,39</sup> The •OH has perfect oxidation ability to degrade MB molecules into CO<sub>2</sub> and H<sub>2</sub>O.

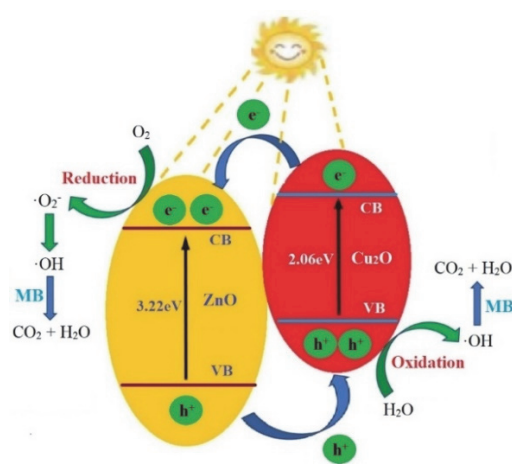


Fig. 8. Possible mechanism of photocatalytic degradation of MB by ZnO/Cu<sub>2</sub>O (S1).

The stability of ZnO/Cu<sub>2</sub>O (S1) was tested by recycling the sample in the photocatalytic degradation experiment of MB. As shown in Fig. 9, after 5 times cycling of photocatalytic degradation,  $R$  only decreased from 98.1 to 92.1 %, indicating that ZnO/Cu<sub>2</sub>O (S1) has good photocatalytic stability.

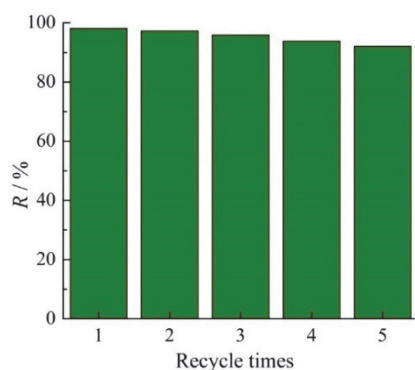


Fig. 9 Recycling experiments of ZnO/Cu<sub>2</sub>O (S1) composite.

#### CONCLUSION

In summary, ZnO/Cu<sub>2</sub>O (S1) nanocomposite was prepared by one-pot method. During the process of preparation, SDS served an effective template. The characterizations confirmed that flower-like ZnO nanoparticles (hexagonal wurtzite) grew on the Cu<sub>2</sub>O nanospheres (cubic crystal) self-assembled from single Cu<sub>2</sub>O particles, and Cu, Zn and O elements were uniformly distributed in the composite. Abundant mesopores were in ZnO/Cu<sub>2</sub>O (S1) and the photo-response range expanded to the visible region. The photocatalytic degradation tests indicated that the degradation ratio  $R$  of MB by ZnO/Cu<sub>2</sub>O (S1) reached 98.1 % after 100 min illumination, significantly larger than that of ZnO (70.0 %), Cu<sub>2</sub>O (36.0 %) and ZnO/Cu<sub>2</sub>O (S2) (80.8 %), and  $R$  did not obviously decrease after 5 recycling, demonstrating high photocatalytic degradation ability and good photocatalytic stability. The enhanced photocatalytic property maybe attributed to the inducement of SDS and the synergy effect of ZnO and Cu<sub>2</sub>O. The advantages of smaller particle sizes, larger amount of meso-pores, more surface adsorption sites, stronger absorption in the visible light range and easier separation of photo-generated carriers ( $e^-/h^+$ ) will help to improve its catalytic degradation ability. The ZnO/Cu<sub>2</sub>O nanocomposite assisted by SDS shows a good application prospect for sewage treatment.

*Acknowledgements.* This work is supported by Anhui Province Young Teacher Training Action: Discipline (Major) Leader Cultivation Project (DTR2023037), Anhui Provincial Teaching Innovation Team (2023cxttd073), Natural Science Foundation of the Department of Education of Anhui Province (2025AHGXZK31414, 2022AH052139), Anhui Engineering Laboratory for Medicinal and Food Homologous Natural Resources Exploration (2025KYPT04) and National/Provincial College Students Innovation Training (202514098035/S202514098176).

The authors extend their gratitude to Mr. Yangjin Zhang (from Scientific Compass [www.shiyanjia.com](http://www.shiyanjia.com)) for providing invaluable assistance with the SEM, XPS and BET analysis.

## ИЗВОД

ПОБОЉШАНА ФОТОКАТАЛИТИЧКА АКТИВНОСТ ZnO/Cu<sub>2</sub>O КОМПОЗИТА ЗА  
РАЗГРАДЊУ МЕТИЛЕН ПЛAVОГ УСЛЕД СИНЕРГИСТИЧКОГ ЕФЕКТА

HONGYING LI,<sup>1,2</sup> LUWEN MA,<sup>1</sup> ZHENYANG WU<sup>1</sup> и CHENGLI YAO<sup>1</sup>

<sup>1</sup>*School of Chemistry and Pharmaceutical Engineering, Hefei Normal University, Hefei, Anhui, China* и <sup>2</sup>*Hefei National Research Center for Physical Sciences at the Microscale, University of Science and Technology of China, Hefei, Anhui, China*

У циљу испитивања каталитичке ефикасности разградње ZnO/Cu<sub>2</sub>O композита, синтетисан је наноккомпозит применом „one-pot“ методе и SDS једињења. Кристална структура, микроскопска морфологија, хемијски састав, специфична површина, расподела величине пора и оптичка апсорпциона својства композита су детаљно окарактерисани. Испитивана је фотокаталитичка активност композита према разградњи метилен плавог (МВ) у присуству зрачења ксенонске лампе. Резултати карактеризације су показали да се синтетисани композит састоји од ZnO (хексагонална вурцитна структура) и Cu<sub>2</sub>O (кубна кристална структура). Захваљујући посредовању SDS једињења, добијене честице су нанометарских димензија, са равномерном расподелом елемената Cu, Zn и O, као и са великим бројем мезопора. Опсег фотокаталитичке активности композита је проширен на видљиви део спектра услед комбинације ZnO и Cu<sub>2</sub>O. Степен разградње МВ једињења у присуству ZnO/Cu<sub>2</sub>O композита износио је приближно 92 % за 100 min након пет поновљених циклуса, што указује на значајан потенцијал за фотокаталитичке примене. Побољшана фотокаталитичка активност може бити повезана са посредовањем SDS једињења током процеса припреме и синергистичким ефектом између ZnO и Cu<sub>2</sub>O.

(Примљено 15. новембра, ревидирано 27. новембра 2025, прихваћено 29. јануара 2026)

## REFERENCES

1. C. Ashina, N. Pugazhenthiran, R. V. Mangalaraja, P. Sathishkumar, *Renew. Sustain. Energy Rev.* **214** (2025) 115490 (<https://doi.org/10.1016/j.rser.2025.115490>)
2. C. Vanlalhmingmawia, H. Moradi, Y. J. Kim, D. S. Kim, J. K. Yang, *Chem. Eng. J.* **509** (2025) 161335 (<https://doi.org/10.1016/j.cej.2025.161335>)
3. C. Q. Shen, X. Y. Li, B. Xue, D. J. Feng, Y. P. Liu, F. Yang, M. Y. Zhang, S. J. Li, *Appl. Surf. Sci.* **679** (2025) 161303 (<https://doi.org/10.1016/j.apsusc.2024.161303>)
4. H. Tu, B. H. Tian, Z. C. Zhao, R. J. Guo, Y. Wang, S. H. Chen, J. Wu, *Water Res.* **28** (2025) 100315 (<https://doi.org/10.1016/j.wroa.2025.100315>)
5. M. Y. Areeshi, *Luminescence* **38** (2023) 1111 (<https://doi.org/10.1002/bio.4432>)
6. H. Y. Li, X. X. Liu, J. Q. Huang, W. J. Zhu, A. M. Ding, C. L. Yao, J. M. Zhu, *Crystallogr. Rep.* **67** (2022) 1231 (<https://doi.org/10.1134/S1063774522070082>)
7. H. Zhao, Z. H. Zhan, W. C. Li, N. Zhang, X. Ma, P. K. Yan, Y. J. Gao, H. L. Cong, Q. Zhang, *J. Alloy. Compd.* **1002** (2024) 175197 (<https://doi.org/10.1016/j.jallcom.2024.175197>)
8. L. Nadjia, A. Chakib, K. Mohamed, T. Mohamed, E. Abdelkader, *Appl. Phys., A* **131** (2025) 154 (<https://doi.org/10.1007/s00339-024-08223-x>)
9. D. Xu, H. L. Ma, *J. Clean. Prod.* **313** (2021) 127758 (<https://doi.org/10.1016/j.jclepro.2021.127758>)

10. A. L. Yang, L. L. Wang, *Curr. Nanosci.* **18** (2022) 94 (<https://doi.org/10.2174/1573413717666210129115305>)
11. R. Rathinabala, R. Thamizselvi, D. Padmanabhan, S. F. Alshahateet, I. Fatimah, A. K. Sibhatu, G. K. Weldegebrieal, S. I. A. Razak, S. Sagadevan, *Inorg. Chem. Commun.* **143** (2022) 109783 (<https://doi.org/10.1016/j.inoche.2022.109783>)
12. P. Attri, S. Garg, J. K. Ratan, A. S. Giri, *Korean J. Chem. Eng.* **41** (2024) 3191 (<https://doi.org/10.1007/s11814-024-00283-2>)
13. J. K. Nie, X. J. Yu, Z. B. Liu, J. Zhang, Y. Ma, Y. Y. Chen, Q. G. Ji, N. N. Zhao, Z. Chang, *J. Clean. Prod.* **363** (2022) 132593 (<https://doi.org/10.1016/j.jclepro.2022.132593>)
14. T. Bekele, G. Mebratie, A. Girma, G. Alamnie, *Colloids Surfaces, A* **685** (2024) 133271 (<https://doi.org/10.1016/j.colsurfa.2023.133271>)
15. X. J. Yu, Z. Y. Li, Z. B. Liu, K. Wang, *Appl. Surf. Sci.* **665** (2024) 160285 (<https://doi.org/10.1016/j.apsusc.2024.160285>)
16. P. Liang, W. Y. Yang, H. Y. Peng, S. H. Zhao, *Molecules* **29** (2024) 5584 (<https://doi.org/10.3390/molecules29235584>)
17. X. S. Wang, Y. D. Zhang, Q. C. Wang, B. Dong, Y. J. Wang, W. Feng, *Sci. Eng. Compos. Mater.* **26** (2019) 104 (<https://doi.org/10.1515/secm-2018-0170>)
18. X. S. Jiang, Q. B. Lin, M. Zhang, G. He, Z. Q. Sun, *Nanoscale Res. Lett.* **10** (2015) 30 (<https://doi.org/10.1186/s11671-015-0755-0>)
19. C. L. Yao, C. Chen, Y. J. Yuan, W. J. Zhu, W. Q. Tai, C. Ding, H. Y. Li, *Cryst. Res. Technol.* **59** (2024) 2300233 (<https://doi.org/10.1002/crat.202300233>)
20. M. Amano, K. Hashimoto, H. Shibata, *J. Oleo. Sci.* **71** (2022) 927 (<https://doi.org/10.5650/jos.ess22061>)
21. J. Cui, L. Ye, X. X. Chen, J. N. Li, B. Yang, M. Yang, Q. Yang, D. Q. Yun, S. D. Sun, *Appl. Surf. Sci.* **638** (2023) 158046 (<https://doi.org/10.1016/j.apsusc.2023.158046>)
22. A. Norouzi, A. Nezamzadeh-Ejhieh, *Mater. Res. Bull.* **164** (2023) 112237 (<https://doi.org/10.1016/j.materresbull.2023.112237>)
23. K. Chitalkar, D. Hase, S. Gurav, S. Musmade, R. Gaikar, M. Sillanpää, V. Murade, H. Aher, *J. Inorg. Organomet. Polym.* **35** (2025) 6961 (<https://doi.org/10.1007/s10904-025-03705-8>)
24. X. J. Yu, J. Zhang, J. Zhang, J. F. Niu, J. Zhao, Y. C. Wei, B. H. Yao, *Chem. Eng. J.* **374** (2019) 316 (<https://doi.org/10.1016/j.cej.2019.05.177>)
25. F. Liu, Y. L. Che, Q. W. Chai, M. F. Zhao, Y. Lv, H. Sun, Y. Q. Wang, J. Sun, C. C. Zhao, *Environ. Sci. Pollut. R.* **26** (2019) 25286 (<https://doi.org/10.1007/s11356-019-05814-7>)
26. Y. W. Lu, F. Yu, J. Hu, J. Liu, *Appl. Catal., A* **429** (2012) 48 (<https://doi.org/10.1016/j.apcata.2012.04.005>)
27. J. K. Nie, X. J. Yu, Z. B. Liu, Y. C. Wei, J. Zhang, N. N. Zhao, Z. Yu, B. H. Yao, *Appl. Surf. Sci.* **576** (2022) 151842 (<https://doi.org/10.1016/j.apsusc.2021.151842>)
28. J. K. Nie, X. J. Yu, Y. C. Wei, Z. B. Liu, J. Zhang, Z. Yu, Y. Ma, B. H. Yao, *Process Saf. Environ.* **170** (2023) 241 (<https://doi.org/10.1016/j.psep.2022.12.002>)
29. T. Nesavi, L. Balu, R. Ezhil Pavai, *Ionics* **31** (2025) 12027 (<https://doi.org/10.1007/s11581-025-06697-0>)
30. J. H. Cao, L. P. Ding, W. T. Hu, X. L. Chen, X. Chen, Y. Fang, *Langmuir* **30** (2014) 15364 (<https://doi.org/10.1021/la5039798>)

31. C. L. Yao, A. J. Xie, Y. H. Shen, W. N. Zhu, J. M. Zhu, *Cryst. Res. Technol.* **49** (2014) 982 (<https://doi.org/10.1002/crat.201400300>)
32. Y. F. Wang, J. Gao, X. Z. Wang, L. P. Jin, L. L. Fang, M. Zhang, G. He, Z. Q. Sun, J. *Sol-Gel Sci. Technol.* **88** (2018) 172 (<https://doi.org/10.1007/s10971-018-4786-8>)
33. N. Akter, T. Ahmed, I. Haque, M. K. Hossain, G. Ray, M. M. Hossain, M. S. Islam, M. A. A. Shaikh, U. S. Akhtar, *Heliyon* **10** (2024) e30802 (<https://doi.org/10.1016/j.heliyon.2024.e30802>)
34. Z. B. Liu, X. J. Yu, K. Wang, J. Zhang, J. F. Niu, *Sep. Purif. Technol.* **356** (2025) 129810 (<https://doi.org/10.1016/j.seppur.2024.129810>)
35. B. Simović, Ž. Radovanović, G. Branković, A. Dapčević, *Mat. Sci. Semicon. Proc.* **162** (2023) 107542 (<https://doi.org/10.1016/j.mssp.2023.107542>)
36. X. J. Yu, J. Zhang, Y. Y. Chen, Q. G. Ji, Y. C. Wei, J. F. Niu, Z. Yu, B. H. Yao, *J. Environ. Chem. Eng.* **9** (2021) 106161 (<https://doi.org/10.1016/j.jece.2021.106161>)
37. H. Usui, *J. Colloid Interface Sci.* **336** (2009) 667 (<https://doi.org/10.1016/j.jcis.2009.04.060>)
38. X. J. Yu, Q. G. Ji, Y. C. Wei, Z. B. Liu, N. N. Zhao, M. Yang, Q. Yang, *J. Electrochem. Soc.* **168** (2021) 126513 (<https://doi.org/10.1149/1945-7111/ac3e79>)
39. S. Y. Gao, J. J. Zhang, W. Q. Li, S. J. Jiao, Y. G. Nie, H. Y. Fan, Z. Zeng, Q. J. Yu, J. Z. Wang, X. T. Zhang, *Chem. Phys. Lett.* **692** (2018) 14 (<https://doi.org/10.1016/j.cplett.2017.11.062>).